Terminal-Terminal Types of Liquid Crystals. III.† Thermal and Electrooptical Behavior of Liquid Crystalline Bis[urethane]s

Kazuo SUGIYAMA,* Koichi KATO, and Kohei SHIRAISHI
Department of Industrial Chemistry, Faculty of Engineering, Kinki University, Takaya, Higashihiroshima, Hiroshima 729-17
(Received December 9, 1991)

Novel terminal-terminal types of liquid crystalline bis[urethane]s **3**, prepared from (*S*)-2-methylbutyl 4-[4-(11-hydroxyundecyloxy)benzylideneamino]cinnamate **2** and various diisocyanates, were studied by differential scanning calorimetry (DSC) and polarized optical microscopy (POM). Bis[urethane]s **3c** obtained from 1,3-diisocyanatobenzene and **3d** from 2,4-diisocyanatotoluene exhibit a smectic state, while bis[urethane]s **3a** obtained from 1,6-diisocyanatohexane, **3b** from bis(4-isocyanatophenyl)methane and **3e** from 2,6-diisocyanatotoluene show no mesophases. It was found from IR spectroscopic results that inter- and intramolecular hydrogen bondings due to N–H and C=O of urethane bonds play an important role in the formation of mesophase. The dual-frequency drive, based on light scattering driven by the application of an a.c. current at different frequencies, was studied in the smectic A state of **3c** and **3d**: τ_r at 0.1 Hz are 0.84 and 0.25 s, τ_r at 1 kHz are 9.75 and 8.95 s for **3c** and **3d**, respectively.

Low molecular weight compounds, comprising two terminal mesogenic groups interconnected by a suitable spacer group may be taken as models for the main-chain type of thermotropic liquid crystalline polymers (TLCPs) which contain core units interconnected through spacer groups.[1–6] The relationship between the structure and liquid crystallinity of such a twin model is known to parallel with that of TLCPs having the same mesogenic units. In spite of much attention given to the structure and phase behavior of the TLCPs of polyester,[7–11] few studies have so far been carried out on the TLCPs of polyurethane.[12–14]

In our previous papers[15,16] we described the synthesis and electrooptical properties of the terminal-terminal type ferroelectric liquid crystals, bis[(*S*)-2-methylbutyl] 3,3′-[ethylenebis(oxy-*p*-phenylenemethylidynenitrilo-*p*-phenylene)]bis[2-propenoate] **1a** [K 157 S_C* 198 S_A 218 N* 245 I] and bis[(*S*)-2-methylbutyl] 3,3′-[icosamethylenebis(carbonyloxy-*p*-phenylenemethylidynenitrilo-*p*-phenylene)]bis[2-propenoate] **1b** [K 122 S_C* 140 S_A 155 I] as twin models for the TLCPs of polyether and polyester. In the present study we prepared five kinds of urethane-based twin models as prototypes of urethane-based TLCPs. We would like to understand the relationship between the structure and property of the twin models in order to obtain useful information for establishing the TLCPs of polyurethane.

Experimental

Preparation of Precursor 2: (*S*)-2-Methylbutyl 4-[4-(11-hydroxyundecyloxy)benzylideneamino]cinnamate **2** was prepared by the reaction of 4-(11-hydroxyundecyloxy)benzaldehyde and (*S*)-2-methylbutyl 4-aminocinnamate in absolute ethanol according to a method described previously.[17]

† For Part II of this series, see Ref. 15.

Preparation of Twin Model 3: Compound **3** was obtained from the reaction of precursor **2** with a variety of diisocyanates, which were heated under reflux in toluene for 24 h. The product was purified by recrystallization from ethanol, followed by column chromatography on silica gel (eluent: petroleum ether). The yield was ca. 80%. Bis[(*S*)-2-methylbutyl] 3,3′-[hexamethylenebis(iminocarbonyloxyundecamethyleneoxy-*p*-phenylenemethylidynenitrilo-*p*-phenylene)]-bis[(*S*)-2-propenoate] **3a**, bis[(*S*)-2-methylbutyl] 3,3′-[methylenebis(*p*-phenyleneiminocarbonyloxyundecamethyleneoxy-*p*-phenylenemethylidynenitrilo-*p*-phenylene)]bis[2-propenoate] **3b**, bis[(*S*)-2-methylbutyl] 3,3′-[*m*-phenylenebis(iminocarbonyloxyundecamethyleneoxy-*p*-phenylenemethylidynenitrilo-*p*-phenylene)]bis[2-propenoate] **3c**, bis[(*S*)-2-methylbutyl] 3,3′-[4-methyl-1,3-phenylenebis(iminocarbonyloxyundecamethyleneoxy-*p*-phenylenemethylidynenitrilo-*p*-phenylene)]bis[2-propenoate] **3d**, and bis[(*S*)-2-methylbutyl] 3,3′-[2-methyl-1,3-phenylenebis(iminocarbonyloxyundecamethyleneoxy-*p*-phenylenemethylidynenitrilo-*p*-phenylene)]bis[2-propenoate] **3e** were characterized by IR, ^{1}H NMR, and elemental analysis, as tabulated in Table 1.

Measurement: ^{1}H NMR measurements were carried out with a 100 MHz JEOL JNM-MH100 spectrometer. IR measurements were carried out with a JASCO IR 810 spectrometer; a heating plate made of aluminum was attached to a temperature controller. For thermal processing IR studies, 5% (W/V) of **3** were dissolved in spectrograde chloroform and poured onto a KBr plate; the solvent was removed in vacuo. The samples were sandwiched between two KBr plates and were used for IR measurements. The phase-transition temperature was determined by DSC with 5 and 10 °C min^{-1} of heating and cooling speed, using a Rigaku Thermoflex apparatus (DSC-8230B). The sample quantity was 5 mg. Polarized optical microscopy (POM) was performed using an Olympus microscope BH-2, with a heating stage attached to a temperature controller. Thin samples were sandwiched between two glass slides, the surface of which had been unidirectionally rubbed with cotton cloth.

Electrooptical measurements were carried out as mentioned previously.[15]

Table 1. Identification of Twin Models **3**

3	^{1}H NMR ($CDCl_3$) δ (ppm)	Elemental analysis/%	C	H	N	IR(KBr) cm^{-1}
3a	5.89—6.24 (d, J=16 Hz, 2H, -CH=CH-), 8.16 (s, 2H, -CH=N-).	$C_{72}H_{102}O_{10}N_4$=1182.760				3335(NH) 1710(C=O), 1690(C=O)
		Found	72.93	8.79	4.69	
		Calcd	73.06	8.69	4.73	
3b	6.00—6.22 (d, J=16 Hz, 2H, -CH=CH-) 7.98 (s, 2H, -CH=N-).	$C_{79}H_{100}O_{10}N_4$=1264.744				3335(NH) 1705(C=O)
		Found	74.62	7.91	4.57	
		Calcd	74.97	7.96	4.43	
3c	6.56—6.92 (d, J=16 Hz, 2H, -CH=CH-), 8.86 (s, 2H, -CH=N-).	$C_{72}H_{94}O_{10}N_4$=1174.700				3430, 3415, 3315(NH) 1725 (C=O),[a] 1705(C=O)
		Found	73.56	8.06	4.77	
		Calcd	73.68	8.13	4.65	
3d	6.37—6.66 (d, J=16 Hz, 2H, -CH=CH-), 8.48 (s, 2H, -CH=NH-).	$C_{73}H_{96}O_{10}N_4$=1189.600				3425, 3400, 3300(NH) 1725(C=O),[a] 1700(C=O)
		Found	73.53	8.21	4.85	
		Calcd	73.71	8.13	4.71	
3e	6.40—6.72 (d, J=16 Hz, 2H, -CH=CH-), 8.54 (s, 2H, -CH=N-).	$C_{73}H_{96}O_{10}N_4$=1189.600				3290(NH) 1705(C=O),[a] 1700(C=O)
		Found	73.62	8.25	4.82	
		Calcd	73.71	8.13	4.71	

a) Hydrogen-bonded C=O stretch.

Results and Discussion

Structure and Properties: Twin models with the structure shown as **3** in Fig. 1 were a pale-yellow powder and were stable to air and prolonged heating at 100 °C. Compounds **3a**, **3b**, and **3e** exhibit a sharp endothermic peak at the melting point in the DSC trace, though precursor **2** shows a mesophase (K 68 S_c* 91 S_A 109 I). Figure 2 depicts the DSC traces at heating and cooling cycles for three twin models: **3c**, **3d**, and **3e**. Twin models **3c** and **3d** show rather broad crystallizing peaks at around 84 and 54 °C with small peaks due to the phase transitions of liquid crystalline–isotropic melts. In the case of **3d**, an appreciably small peak, other than two well-defined peaks, was observed at 65 °C, and is assumed to be due to the phase transition of the S_A-unknown S phase.[18] Twin model **3d** shows a lower, wider S_A phase than does **3c**, since **3d** has a methyl group that is unsymmetrical adjacent to two urethane linkages. On the other hand, **3e** shows a very sharp peak at around 102 °C. According to POM, **3c** and **3d** show an enantiotropic S_A phase having a focal conic texture. The phase-transition temperature of the samples determined using DSC is compatible with that obtained by means of POM and electrooptical measurements, as tabulated in Table 2. Differences in the

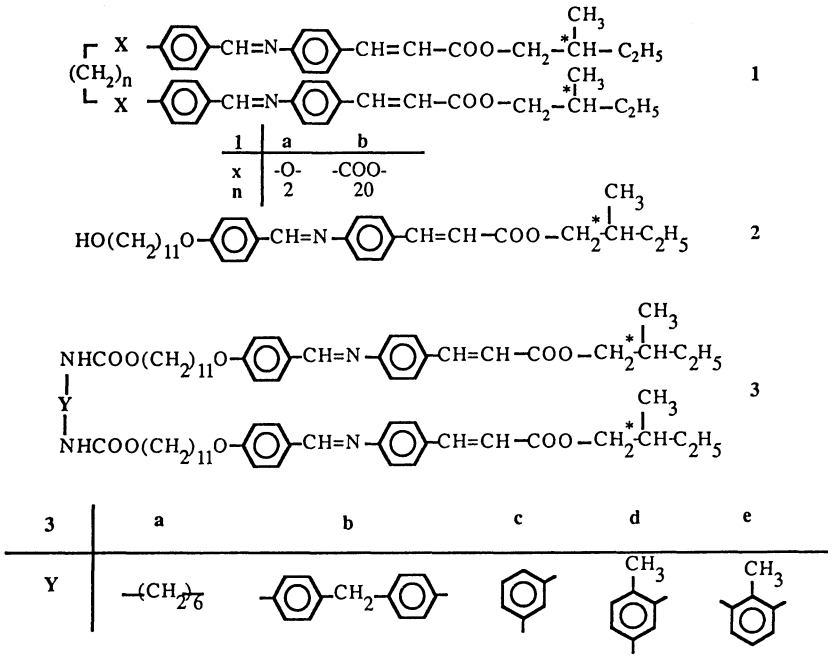

Fig. 1. Structure of terminal–terminal types of liquid crystals.

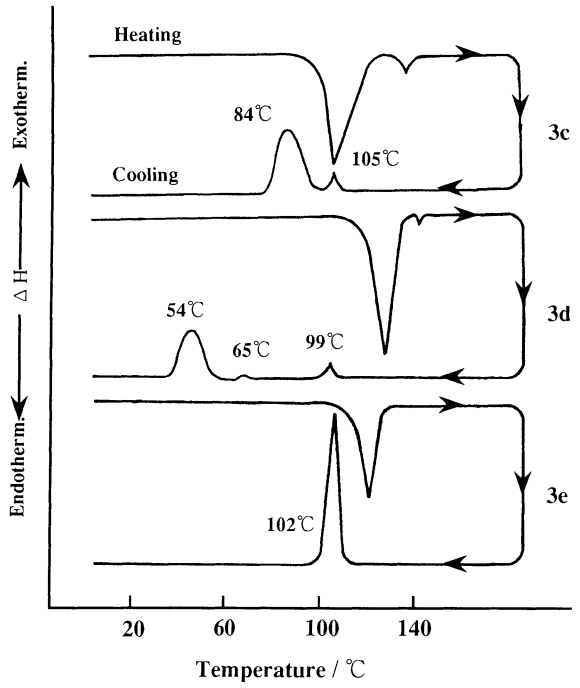

Fig. 2. DSC traces of twin models **3c**, **3d**, and **3e**.

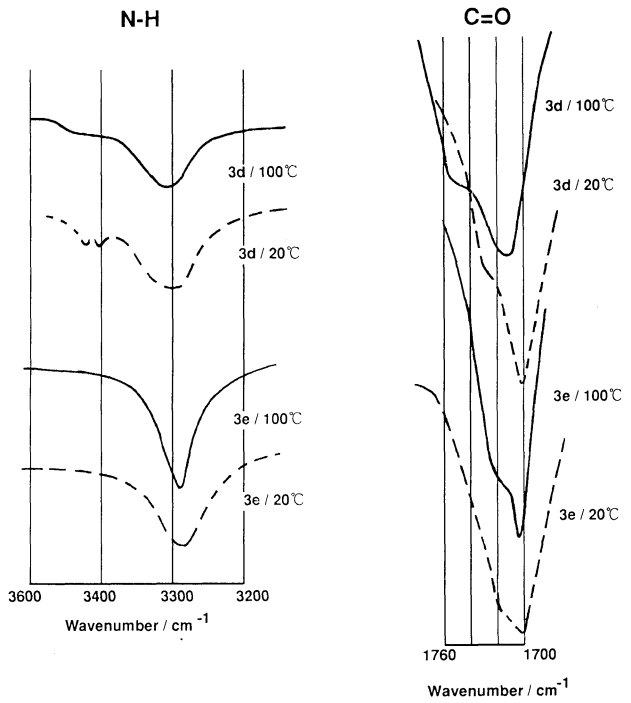

Fig. 3. IR spectra of N–H and C=O stretching vibration for twin models **3d** and **3e** at various temperatures, (——)**3d**; (----)**3e**.

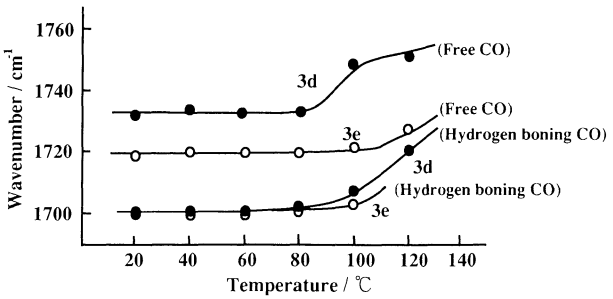

Fig. 4. Temperature dependence of the C=O stretching band for twin models **3d** and **3e**, (●), **3d**; (○), **3e**.

thermal behavior of **3c**, **3d**, and **3e** provide important information concerning the preparation of urethane-based TLCPs. For the development of the liquid crystalline state, the intermolecular interactions are limited to exclude volume effects and dispersive forces.[19] In twin model **1b**, for instance, the rigid core unit tends to self-associate by an intermolecular interaction; a reasonably long aliphatic chain contributes to the formation of the mesophase, especially an S_C^* phase. In addition to the structural differences of the mesogenic groups, a hydrogen bonding interaction plays an important role to form mesophases. Thermal processing IR measurements provided interesting information concerning the interaction based on hydrogen bondings. Figure 3 shows the typical IR spectra of **3d** and **3e** as a function of the temperature, including the main features of the N–H stretch in the 3200—3600 cm^{-1} region and the C=O stretch in the 1700—1760 cm^{-1} region. It has been known that the frequencies and relative intensities of the C=O and N–H vibrations are characteristic of hydrogen-bond formation.[13] Since N–H and C=O stretching vibrations of **3e** appear at lower frequencies than do those of **3d**, it is suggested that the intermolecular hydrogen bonding of **3e** is stronger than that of **3d**. Figure 4 describes the effect of temperature on the intensity of the C=O stretching band in the range of 20 to 120 °C. The stretch regarded as free C=O appears at

Table 2. Transition Temperatures, Enthalpies and Entropies of Model **2** and Twin Models **3**[a]

Compound	Phase transition temperature of **3**/°C	$\Delta H^{a)}$/kJ mol^{-1}		$\Delta S^{a)}$/J mol^{-1} K^{-1}		Phase-transition temperature of **3** and DOBAMBC system/°C
		T_m	T_i	T_m	T_i	
2	K 68 S_C^* 91 S_A 109 I	27.5	4.8	81.1	12.9	—
3a	K 123 I	81.3	—	206.3	—	Immissible
3b	K 120 I	73.4	—	190.2	—	Immissible
3c	K 84 S_A 105 I	51.8	5.0	142.1	13.4	K 38 S_A 89 I
3d	K 54 S_X 65 S_A 99 I	39.2	4.9	124.6	13.3	K 25 S_C^* 53 S_A 93 I
3e	K 102 I	47.7	—	127.6	—	Immissible

a) ΔH and ΔS were calculated from the area of cooling trace.

1725 and 1715 cm^{-1} for **3d** and **3e**, respectively. It was also found that two C=O stretch bands of **3e** gradually shift to a higher frequency region with increasing temperature above the melting point, while a significant change of frequencies occurs in **3d** below the S_A–I transition. These facts indicate that in the case of **3d**, intramolecular hydrogen bonding is a predominant factor in the development of the mesophase. Intramolecular hydrogen bonding should exist in **3d** as is shown in Fig. 5. Accordingly, the intermolecular interaction due to hydrogen bonding in **3c** and **3d** is not so strong that the molecules could develop the mesophase, due to exclude volume effects and dispersive forces. The structure (shown as Fig. 5) also describes the smooth formation of the S_A state in **3c** and **3d** since two mesogenic groups are closely aligned to each other so as to orient the dipoles in the same direction. In contrast, since intermolecular hydrogen bonding is the dominant factor in crystallization, **3e** exhibits the transition of K–I alone. The thermal behavior of **3a** and **3b** may be interpreted in the same way, since their C=O and N–H vibration appear at lower frequencies than those of **3c** and **3d**, as shown in Table 1. Though X-ray analyses of these twin models have not yet been undertaken, twin models **3c** and **3d** are, thus, anticipated to be a folded-form, while **3e** may be taken as an unfolded-form, due to the methyl group between the two urethane linkages. Unfolded forms **3a**, **3b**, and **3e** would also be favorable for crystallization. In order to reinforce these results, mixed liquid crystals of **3** and DOBAMBC[20] (molar ratio 1 : 1) were prepared and tested thermally. Twin models **3c** and **3d** are completely miscible with DOBAMBC, and the mixed liquid crystals show lower and wider mesophases than do **3** and DOBAMBC, themselves, as shown in Table 2. On the other hand, **3a**, **3b**, and **3e** are immiscible with DOBAMBC, and the mixtures show a phase segregation which is realized by POM. It is explained that the molecules of **3a**, **3b**, and **3e** can easily aggregated themselves to form their own domains by intermolecular hydrogen bonding; they cannot mix uniformly with DOBAMBC in molecular size.

Electrooptical Properties: Since **3c** and **3d** show the S_A state, the twin models were measured on a dual-frequency drive based on light scattering under two different conditions of an a.c. electric field in the S_A state in order to obtain basic data for practical use. The sample was sandwiched between ITO-coated glass plates (cell thickness=25 μm). A change in the transmission intensity (T) of the He–Ne laser through the cell with the application of an a.c. field was detected by means of a photodiode and recorded with digital storage oscilloscope. Figure 6 shows the change in T due to applying different conditions of an a.c. electric field in the S_A state of **3d**. Upon application of an a.c. electric field of 0.1 Hz (electric field E=48 kV cm^{-1}) in the S_A state, T strikingly decreased within one second. When the electric field was removed, T gradually increased up to the original intensity. On the other hand, upon applying an a.c. field of 1 kHz (E=48 kV cm^{-1}), T gradually increased. In the case of applying a low-frequency field, a decrease of T was observed based on light scattering caused by the collapse of a well aligned S_A layer due to a turbulent flow by an ionic current caused by a small amount of impurities contained in the sample.[21] When a high-frequency field was applied, the molecules reorient in the S_A state with a homeotropic alignment, due to the dielectric characteristics, since an ionic current was induced. From Fig. 6, the response time (τ_{lr}) due to the transition from homeotropic alignment to the collapsed state, and the response time (τ_{hr}) due to the reverse change, were measured. A similar electrooptical response was observed with other samples. In this measurement, the response time was conventionally defined as being the time period taken to reach the stage of a T decrease up to 90% of the original intensity of the S_A state.

The results of the electrooptical effect are summarized in Table 3. We believe that information concerning the thermal and electrooptical properties of twin models obtained here is useful for building up TLCPs of polyurethane. From the results concerning the thermal and electrooptical properties of urethane-based twin models, the following conclusions can be drawn:

1. Twin models **3a**, **3b**, and **3e** show transition alone, whereas **3c** and **3d** exhibit a smectic mesophase.
2. Hydrogen bonding plays an important role in

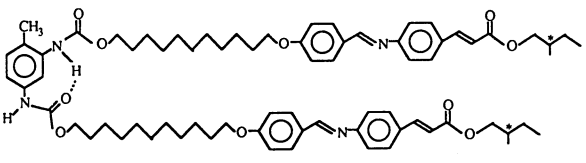

Fig. 5. Schematic illustration of intramolecular hydrogen bonding of twin model **3d**.

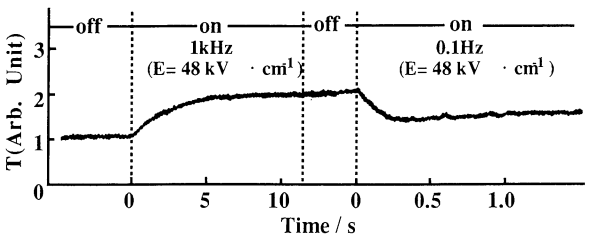

Fig. 6. Response time (τ_r) in the S_A phase of twin model **3d** at 120 V (E=48 kV cm^{-1}) at 87 °C.

Table 3. Electrooptical Effects of Twin Models **3**

Compound	Response time[a]/s	
	τ_{lr}/ at 0.1 Hz	τ_{hr}/ at 1 kHz
2	0.71	10.0
3c	0.84	9.75
3d	0.25	8.95

a) τ_r was measured at $T_{I\text{-}S_A}$–10 °C, 120 V of a.c.

phase transition of bis[urethane]s.

3. The S_A phase in **3c** and **3d** show a dual-frequency drive based on light scattering driven by the application of an a.c. current at different frequencies.

References

1) R. B. Blumstein, M. D. Poliks, E. M. Stickles, A. Blumstein, and F. Volino, *Mol. Cryst. Liq. Cryst.*, **129**, 375 (1985).

2) H. Toriumi, H. Furuya, and A. Abe, *Polym. J.*, **17**, 895 (1985).

3) J. C. W. Chien, R. Zhou, and C. P. Lillya, *Macromolecules,* **20**, 2340 (1987).

4) P. Esnault, D. Galland, F. Volino, and R. B. Blumstein, *Mol. Cryst. Liq. Cryst. Inc. Nonlin. Opt.*, **157**, 409 (1988).

5) A. C. Griffin, S. L. Sullivan, and W. E. Hughes, *Liq. Cryst.*, **4**, 409 (1988).

6) G. S. Attard, S. Garnett, C. G. Hickman, C. T. Imrie, and L. Taylor, *Liq. Cryst.*, **7**, 495 (1990).

7) T. Uryu and T. Kato, *Macromolecules,* **21**, 378 (1988).

8) S. Brückner, *Macromolecules,* **21**, 633 (1988).

9) S. Hu, M. Xu, J. Li, B. Qian, X. Wang, R. W. Lenz, and R. S. Stein, *Polymer,* **29**, 789 (1988).

10) A. Yu. Bilibin, A. V. Tenkovtsev, and O. N. Piraner, *Makromol. Chem.*, **190**, 3013 (1989).

11) S. Hu, M. Xu, J. Li, B. Qian, K. Tao, and R. W. Lenz, *J. Polym. Sci.: Part B: Polym. Phys.*, **27**, 1749 (1989).

12) S. K. Pollack, G. Smyth, P. J. Stenhouse, F. Papadimitrakopoulos, S. L. Hsu, S. J. Kantor, and W. J. Macknight, *Polym. Prepr. (Am. Chem. Soc., Div. Polym. Chem.)*, **30(2)**, 517 (1989).

13) S. K. Pollack, D. Y. Shen, S. L. Hsu, Q. Wang, H. D. Stidham, *Macromolecules,* **22**, 551 (1989).

14) P. J. Stenhouse, E. M. Valles, S. W. Kantor, and W. J. Macknight, *Macromolecules,* **22**, 1467 (1989).

15) K. Shiraishi, K. Kato, and K. Sugiyama, *Bull. Chem. Soc. Jpn.*, **63**, 1848 (1990).

16) K. Shiraishi, K. Kato, and K. Sugiyama, *Chem. Lett.*, **1990**, 971.

17) K. Sugiyama, K. Kato, and K. Shiraishi, *Bull. Chem. Soc. Jpn.*, **64**, 1652 (1991).

18) According to POM around 65 °C, the texture of the mesophase differs from that of S_A phase but it is not known to which S phase do it belong at present.

19) H. Finkelmann, *Angew. Chem., Int. Ed. Engl.*, **26**, 816 (1987).

20) (*S*)-2-methylbutyl 4-[4-(decyloxy)benzylideneamino]-cinnamate: S_H 63 S_C* 95 S_A 118 I: R. B. Meyer, L. Liebert, L. Strzelecki, and P. Keller, *J. Phys. Lett.*, **36**, L269 (1978).

21) T. Kajiyama, H. Kikuchi, A. Miyamoto, S. Moritomi, and J. C. Hwang, *Chem. Lett.*, **1989**, 817.